ACS APPLIED MATERIALS & INTERFACES

Research Article

www.acsami.org

Effect of Octa(aminophenyl) Polyhedral Oligomeric Silsesquioxane Functionalized Graphene Oxide on the Mechanical and Dielectric Properties of Polyimide Composites

Wei-Hao Liao, Shin-Yi Yang, Sheng-Tsung Hsiao, Yu-Sheng Wang, Shin-Ming Li, Chen-Chi M. Ma,* Hsi-Wen Tien, and Shi-Jun Zeng

Department of Chemical Engineering, National Tsing-Hua University, Hsin-Chu 30013, Taiwan

Supporting Information

ABSTRACT: An effective method is proposed to prepare octa(aminophenyl) silsesquioxane (OAPS) functionalized graphene oxide (GO) reinforced polyimide (PI) composites with a low dielectric constant and ultrastrong mechanical properties. The amine-functionalized surface of OAPS-GO is a versatile starting platform for in situ polymerization, which promotes the uniform dispersion of OAPS-GO in the PI matrix. Compared with GO/PI composites, the strong interfacial interaction between OAPS-GO and the PI matrix through covalent bonds facilitates a load transfer from the PI matrix to the OAPS-GO. The OAPS-GO/PI composite film with 3.0 wt % OAPS-GO exhibited an 11.2-fold increase in tensile strength, and a 10.4-fold enhancement in tensile modulus compared with neat PI. The dielectric constant (D_k) decreased with the increasing content of 2D porous OAPS-GO, and a D_k value of 1.9 was achieved.

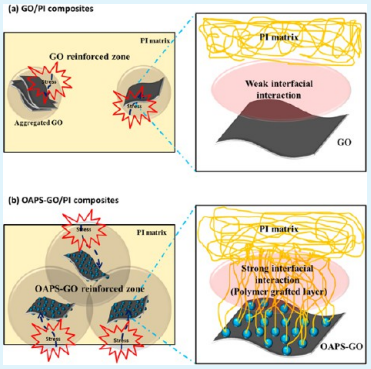

KEYWORDS: *graphene oxide, octa(aminophenyl) POSS, polymer-matrix composites (PMCs), mechanical properties, dielectric properties*

1. INTRODUCTION

Polymer composites with graphene-based nanofillers have generated substantial academic and industrial interest, because of their potential applications, which include thermal management, fuel cells, and use in low-dielectric-constant materials.[1−4] Previous reports[5,6] have investigated the improvement of polymer properties by incorporating graphene-based materials. The actual performances of these composites were lower than the anticipated values, which had been estimated based on the ultrahigh surface area and superior mechanical properties of graphene. The reinforcing efficiency between the graphene-based materials and the polymer matrix was reduced, since graphene-based materials were restacked and aggregated.[5,6] Two major factors limit the reinforcing efficiency of nanofillers in the polymer matrix, which are (1) the poor dispersion of nanofillers in the polymer matrix, and (2) the weak interfacial interactions between the nanofillers and the polymer matrix.[2,7,8] Consequently, improving the dispersibility of nanofillers in a polymeric matrix and providing strong interfaces between the nanofillers and a polymer matrix to obtain high-performance composites are critical and indispensable issues.[9−15]

Graphene-based materials, such as graphene nanosheets (GNSs) and graphene oxide (GO), exhibit great potential for improving the properties of polymer composites because of their extraordinarily high surface area, unique graphitized planar structure, and low manufacturing cost.[16−18] GO is different substantially from GNSs considering chemical structure, leading to a great potential for further functionalization. GO consists of a two-dimensional sheet of covalently bonded carbon atoms bearing various oxygen functional groups (e.g., hydroxyl, epoxide, and carbonyl groups) on the basal planes and edges. The oxygen functional groups on the GO surface provide electrical insulation and versatile sites for chemical functionalization, improving the compatibility, and enhancing the dispersion of GO in polymeric matrices.[17,19] Furthermore, by designing functionalized GO with a specific chemical structure that can form covalent bonds with a specific polymeric matrix to strengthen the interfacial interaction between GO and the polymer host.[2,20,21]

Polyhedral oligomeric silsesquioxane (POSS) is another noteworthy nanomaterial for reinforcing polymers in composites, due to its unique cagelike molecular structure and physicochemical properties. Typical POSS cages are represented by the formula $(RSiO1.5)n$, where R represents hydrogen or various functionalized groups. POSS cages consist of Si−O inorganic bonds, Si atoms at the eight top angles of the cube structure bridging with O atoms, and eight substitutive groups R on the Si atom.[22,23] Consequently, nanoporous POSS cages with functionalized substituents have been studied in previous reports[24−26] to improve polymer properties. These

Received: May 12, 2014
Accepted: August 25, 2014
Published: August 25, 2014

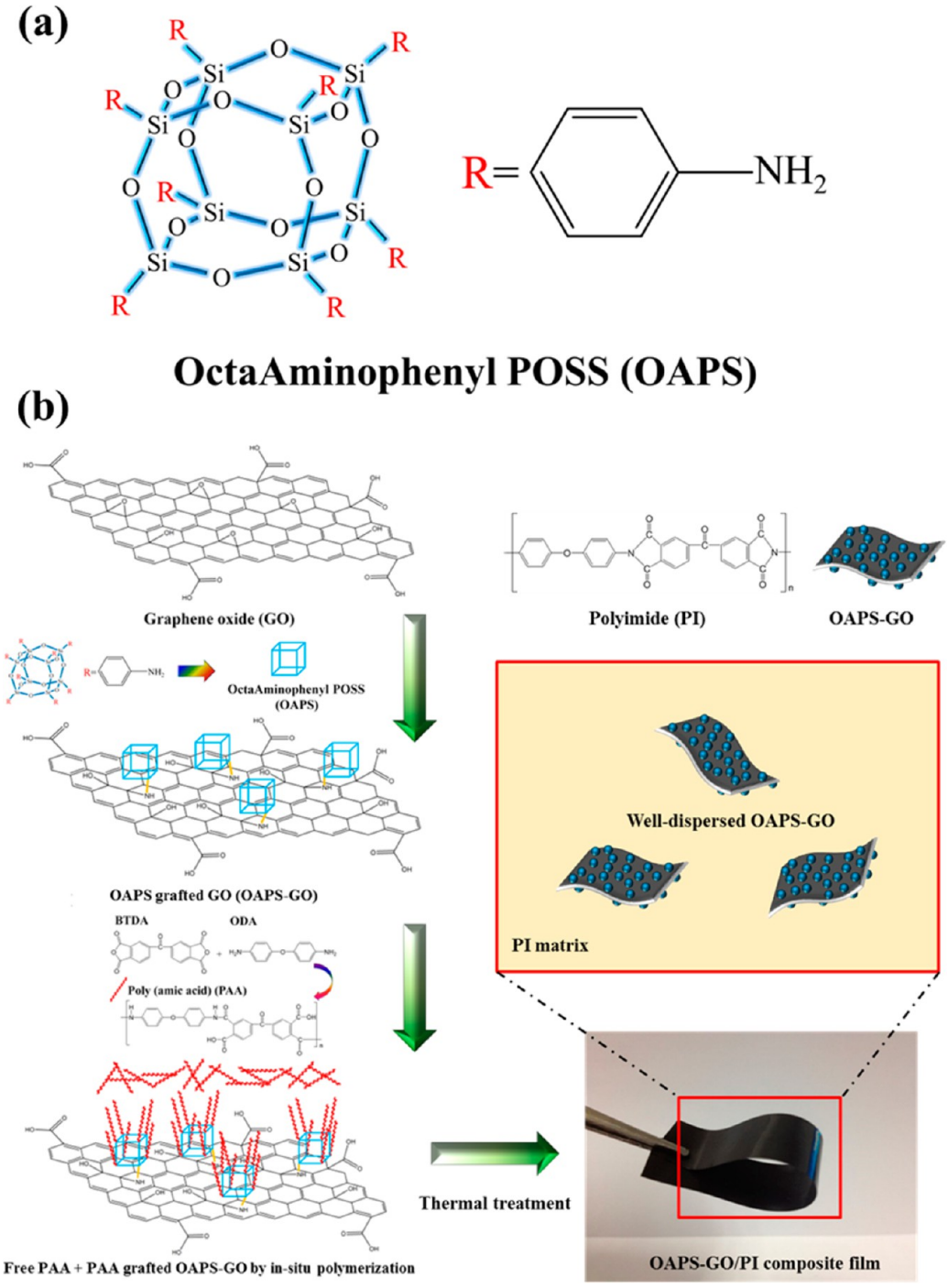

Figure 1. (a) Structure of OAPS, and (b) scheme of the procedure for preparation of OAPS-GO/PI composites.

POSS reinforcements have substantially enhanced the mechanical properties, thermal behavior, flame retardancy, and particularly, the low dielectric constant of polymers.[24,27]

With the growing demand for portable communication system, such as laptop, tablet computer, and smartphone, the development of ultralarge-scale integration (ULSI) processes has exhibited a trend toward minimizing the dimensions and enhancing the integration density of integrated circuit (IC) devices.[28] The numbers of interconnects in ICs are continuously increasing, resulting in electronic signal interference (noise, crosstalk, and power dissipation) caused by parasitic resistance and capacitance delays (RC delay).[29] To solve this problem, low-dielectric-constant materials have been used to provide an interlevel metal insulator, which has attracted the interest of scientists and the semiconductor manufacturing industry.[29,30] The International Technology Roadmap for Semiconductors (ITRS) requires interlayer dielectric (ILD) materials to possess bulk dielectric constants (D_k) below 2.4 and tensile strength above 200 MPa for constructing an IC structure.[31]

Polymer-based ILD materials have attracted academic and industrial attention because of their low cost and excellent processability.[28] However, the electrical properties of these materials do not meet the current ILD requirements for ULSI

multilevel interconnections. Because the D_k of air is approximately 1.0, the most convenient method for decreasing the D_k is to construct materials that possess a porous structure. However, the mechanical properties of porous materials are typically too weak for ILD material applications.[32,33] Moreover, designing a material with a molecular structure involving fluorine-containing groups can reduce the D_k value. The dielectric constants of fluorinated polymers are low (e.g., fluorinated polyimide, D_k 2.6−2.8), however, they also suffer from poor mechanical properties and high monomer cost.[28,34] Previous reports[26,33−35] have proposed promising approaches to reduce the dielectric constants of materials, without sacrificing their mechanical properties, such as incorporating insulating nanofillers in the polymeric matrices. Among polymer-based ILD materials, polyimides (PI) exhibit the greatest promising potential to be a based polymer for the ILD materials, because PI possesses high thermal stability, excellent mechanical properties, and unique dielectric properties with D_k values in the range from 3.2 to 3.9.[28] However, these D_k values of PI do not meet current ILD requirements. To reduce the dielectric constant of PI-based material, previous studies have demonstrated that using some nanofillers, such as silica/PI,[35] clay/PI,[36] POSS/PI,[37] and GO/PI,[38] to reinforce PI for manufacturing composites can reduce the dielectric constants of these materials and enhance the mechanical properties of the PI efficiently.

Despite certain studies[39−42] reporting that the POSS with a single amine-functionalized group was grafted onto the GO surface by forming covalent bonds, using POSS-grafted GO sheet as a nanofiller in polymeric composites has seldom been investigated. Recently, Wenqi Yu et al.[38] synthesized octa-(aminophenyl)-polyhedral-oligomeric-silsesquioxanes (OAPS)-functionalized GO (OAPS-GO), and investigated the dielectric properties of OAPS-GO/epoxy composites. Compared with their report, this study not only investigated the dielectric properties of the OAPS-GO/PI composites, but also provided a framework for studying the interfacial interaction between GO and OAPS-GO and the PI polymeric matrix by investigating the mechanical properties of the GO/PI and OAPS-GO/PI composites. On the basis of a review of the literature, few reports have focused on the application of a multiamine-functionalized OAPS-GO nanomaterial as a reinforcement material in PI composites.

Compared to disperse pristine GO in the polymeric matrix, the grafting OAPS on the GO sheets serves as intercalator between GO interlayers to prohibit the aggregation and restacking of the GO sheets in the polymeric matrix. In addition, The OAPS-GO surface provides amine functional groups as reactive sites for grafting poly(amic acid) (PAA) during the in situ polymerization. The OAPS-GO/PAA composites were imidized by the thermal treatment, forming the OAPS-GO/PI composite films, which obtained a strong interfacial interaction between OAPS-GO and the PI matrix. Compared with the neat PI film, the OAPS-GO/PI composite films exhibited a significant improvement in mechanical properties. The dielectric constant (D_k) decreased with the increasing content of GO; the D_k of the OAPS-GO/PI composite film was as low as 1.9. Consequently, the proposed approach provides a promising path for developing high-performance OAPS-GO/PI composite materials for next-generation low-*k* dielectric materials.

2. EXPERIMENTAL SECTION

2.1. Materials. 4,4′-Diaminodiphenyl ether (ODA) was obtained from TCI America, Portland, Oregon, USA. 3,3′,4,4′-Benzophenone-tetracarboxylic dianhydride (BTDA) was obtained from Aldrich Chemical Co., St. Louis, MO, USA. The purity of ODA was greater than 99%, and the purity of BTDA was above 98%. Moreover, vapors of ODA and BTDA monomers were removed in a vacuum oven before the PAA-synthesis reaction. OAPS (as shown in Figure 1a) was received from Hybrid Plastics (Hattiesburg, Mississippi, USA) and was used as received. Nano Graphites (NGPs) were supplied by Angstron Materials LLC, McCook Avenue, Dayton, Ohio, USA, and was produced by a chemical vapor deposition (CVD) process. The thickness of the NGPs was smaller than 100 nm. Potassium permanganate ($KMnO_4$), sodium nitrate ($NaNO_3$), dimethylacetamide (DMAc), and sulfuric acid (H_2SO_4) were received from the Showa Chemical Co., Tokyo, Japan.

2.2. Preparation of GO. On the basis of Hummers method,[43] H_2SO_4 (50 mL) was poured into a 250 mL three-neck flask and stirred in an ice bath and the temperature was maintained at 0 °C. NGPs (2 g) and $NaNO_3$ (1 g) were added and stirred uniformly. $KMnO_4$ (6 g) was slowly added to the mixture over the course of 30 min with the reaction vessel in an ice bath. The solution was then heated to 35 °C and oxidation was allowed to proceed for 24 h. Distilled water then was added slowly, and the temperature was controlled below 100 °C. This reaction was terminated by adding a large quantity of distilled water and 30% H_2O_2 solution (6 mL). The mixture was filtered and washed with distilled water. This process was repeated at least ten times until the pH of the percolated solution reached 7. The sample of GO was obtained after drying in a vacuum oven.

2.3. Preparation of GO/PI Composite Films by Solution Blending Method. To synthesize PAA, we placed 2.0 g of ODA (0.02 mol amine group) in a three-neck flask containing 20 mL of DMAc under a nitrogen purge at room temperature. After ODA was completely dissolved in DMAc, 3.2 g of BTDA (0.02 mol anhydride group) was divided into four batches. Each batch was then added to the three-neck flask every 2 h. After BTDA was completely dissolved in DMAc, the solution was stirred for 10 h, and a viscous PAA solution was obtained. For purification, the PAA solution was fed into a dialysis membrane (Nominal MWCO: 6000−8000, Cellu•Sep Regenerated Cellulose Tubular Membranes, Belgium), and immersed in pure DMAc for 8 h. To prepare GO/PI composite films with distinct concentrations, various contents of GO (0.5, 1.0, 3.0, and 5.0 wt %) were added to 10 mL of DMAc individually, and each sample was then dispersed in DMAc through sonication. The dispersed GO suspensions were then mixed with PAA to prepare GO/PAA mixtures through blending in DMAc. Theses GO/PAA mixtures were then poured into a glass dish, and the residual solvent was removed using vacuum evaporation at 30 °C for 1 h. For imidizing the GO/PAA mixtures, the samples were placed in a convection oven at 100, 150, 200, and 300 °C for 2 h and then at 400 °C for 5 min. The film thickness was controlled at 0.1 mm.

2.4. Preparation of OAPS-GO/PI Composite Films by in Situ Polymerization Process. Figure 1(b) depicts the procedure for preparing OAPS-GO/PI composite films. GO (16.6 mg, approximately 0.10 mmol epoxide group and 0.025 mmol carboxylic group (a detailed estimation is available in the Supporting Information)) was dispersed in anhydrous DMAc (10 mL), through sonication leading to disperse GO in solution uniformly. GO solution was then placed in a 100 mL three-necked flask, which was equipped with a magnetic stirrer, and a nitrogen inlet and outlet. Simultaneously, OAPS (144.1 mg, 0.995 mmol amine functional group) was dispersed in 10 mL of DMAc through sonication, and the OAPS solution was also added to the three-necked flask reactor. The mixture was refluxed and stirred at 60 °C for 24 h in a nitrogen atmosphere, and the OAPS-functionalized GO was assigned as OAPS-GO. After the OAPS-functionalized GO was produced, it was washed using 1L of DMAc solvent, and filtered by a membrane filter (hydrophilic PTFE membrane filters, pore size: 0.1 μm, Advantec membrane filter, USA) and a vacuum filtration process. Subsequently, ODA (2g, 20 mmol amine functional group) were placed in the reactor. After ODA was completely dissolved in

DMAc, BTDA (3.36 g, 20.87 mmol anhydride functional group) was divided into four batches. Each batch was then added to the three-neck flask every 2 h at room temperature. After BTDA was completely dissolved in DMAc, the solution was stirred for 10 h at room temperature, and a viscous OAPS-GO/PAA solution was obtained. The mixture was then poured into a glass dish, followed by vacuum evaporation at 30 °C for 1 h and thermal treatment at 100, 150, 200, and 300 °C for 2 h and then at 400 °C for 5 min. The OAPS-GO/PI composite films containing 0.5, 1.0, 3.0, and 5.0 wt % OAPS-GO were prepared using the above-mentioned experimental steps. The film thickness is controlled at 0.1 mm.

2.5. Characterization and Instruments. A high-resolution X-ray photoelectron spectrometer (XPS) (ESCA pHI 1600, Physical Electronics, Lake Drive East, Chanhassen, MN, USA) was used to detect the presence of surface elements.Transmission electron microscope (TEM) observations were conducted using a JEM-2100 microscope (JEOL Limited, Tokyo, Japan) with 200 kV. An Ultima IV multipurpose X-ray diffraction (XRD) system (Rigaku Co., Sendagaya, Shibuya-Ku, Tokyo, Japan) was used for the X-ray analysis with Cu Kα radiation (λ = 1.54051 Å). Step scanning was used with 2θ intervals from 2° to 35° with a residence time of 1 s. Thermogravimetric analyses (TGA) were performed with a Du Pont TGA 2900 analyzer from 30 to 800 °C in air at a heating rate of 10 °C min^{-1}. The scanning electron microscope (SEM) used in this work was a Hitachi S-4200 SEM (Hitachi Limited, Tokyo, Japan) with an accelerating voltage of 15 kV. To measure the tensile strength and modulus of the PI films, samples were cut to sheets with a width of 10 mm, and were tested using an Universal Testing Machine (Tinius Olsen H10K−S Benchtop Testing Machine, Horsham, PA, USA). The test procedure followed the ASTM-D882. Dimensions of test specimen were 50 mm × 5 mm × 0.1 mm; the crosshead speed was 5 mm min^{-1}. The dielectric constants of OAPS-GO/PI films were measured over a frequency range from 0.01 to 1.0 GHz at room temperature using a dielectric spectrometer (Hewlett-Packard 4291A RF Impedance Analyzer).

3. RESULTS AND DISCUSSION

3.1. Characterization of GO and OAPS-GO. A high-resolution XPS was used to detect the surface composition and functional groups of GO and OAPS-GO based on the chemical shift observations. Survey scans were conducted to investigate the element composition of the surface of the sample. The XPS survey spectra of GO and OAPS-GO are presented in Figure 2. GO exhibits a significantly intense O 1s peak, resulting from the presence of oxygen-containing groups on the GO surface. After functionalization, OAPS-GO exhibited the additional N 1s, Si 2s, and Si 2p peaks compared with GO, which were attributed to the composition of the grafted OAPS on GO, confirming the success of the modification.

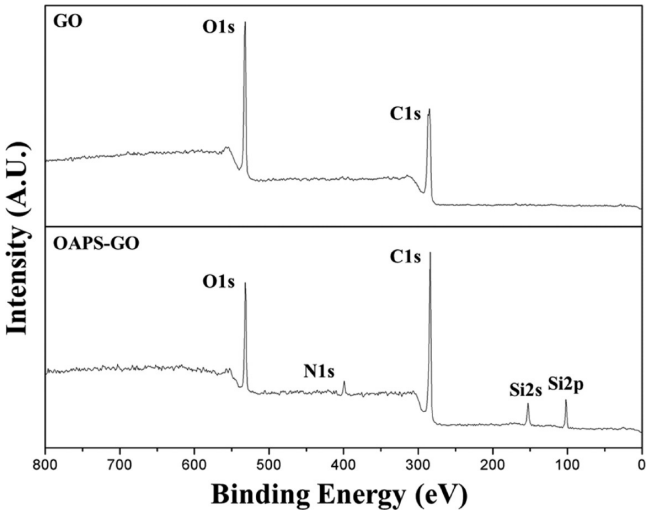

Figure 2. XPS survey scans of GO and OAPS-GO.

To provide further evidence of OAPS being grafted on the GO surface, a detailed analysis of the C 1s XPS spectra are shown in Figure 3. The C 1s XPS spectrum of GO showed that

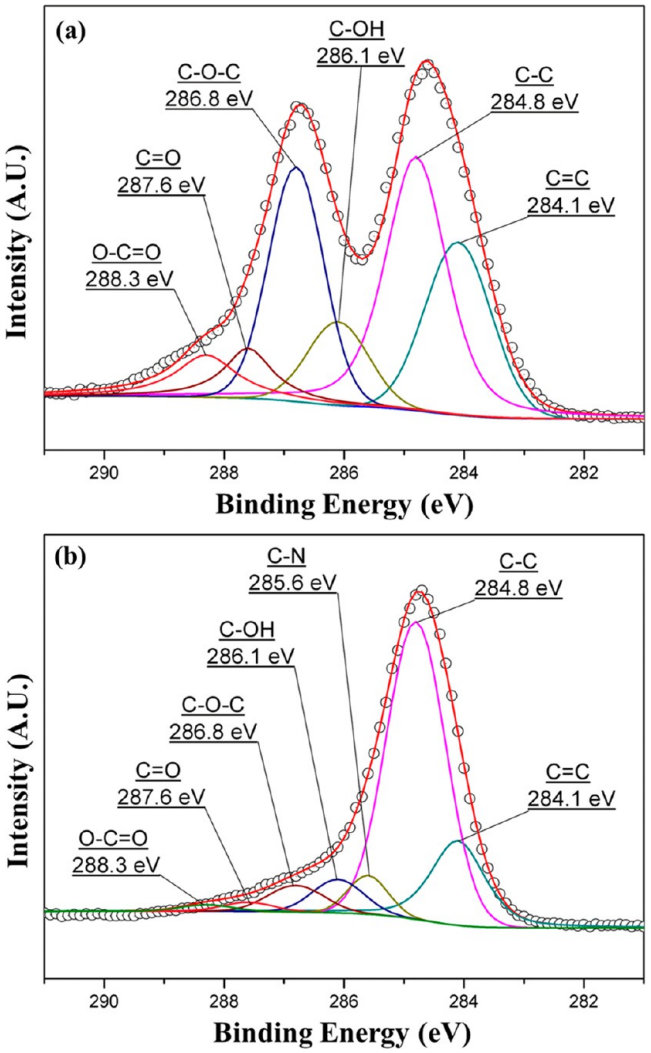

Figure 3. C 1s XPS spectra of (a) GO and (b) OAPS-GO.

the as-prepared GO possesses a considerable degree of oxidation since the numerous oxygen-functionalities such as C−OH (286.1 eV), C−O−C (286.8 eV), C═O (287.6 eV), and O−C═O (288.3 eV) were observed.[17,44] These oxygen-functional groups result in GO exhibiting excellent potential for chemical modification. Compared with GO, the C 1s XPS spectrum of OAPS-GO exhibited an additional peak at 285.6 eV, originating from the C−N bonds,[11,44] and the peaks of the epoxide group and carboxylic group decreased obviously. These results indicate that the OAPS attaches to the surfaces of GO through a nucleophilic attack, which is a ring-opening reaction occurring between the amine groups of OAPS and the epoxy groups on the GO surface, forming the C−N covalent bonds.

To characterize the morphologies of GO and OAPS-GO further, we used TEM to observe the morphology of the structures (as shown in Figure 4). The GO sheet (as shown in

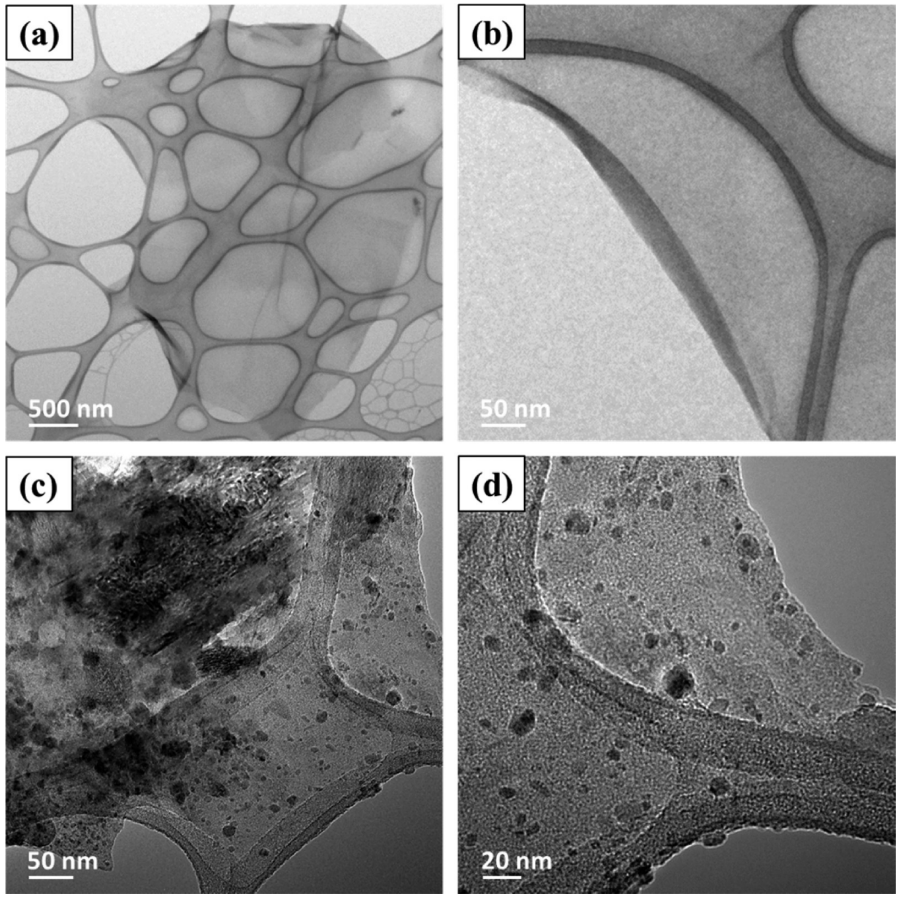

Figure 4. TEM images of (a) GO at low magnification, (b) GO at high magnification, (c) OAPS-GO at low magnification, and (d) OAPS-GO at high magnification.

Figure 4a, b) possessed a high density of oxygen-containing functional groups on the surface, and exhibited a smooth carpetlike structure. Compared with GO, OAPS-grafted GO exhibited a rougher structure (as shown in Figure 4c). OAPS particles were deposited on the GO surface (as shown in Figure 4d), suggesting the successful grafting of OAPS onto GO. OAPS-GO exhibited unique 2D nanostructures and large aspect ratios that could enhance their contact areas within the polymeric matrix. This is an important potential for improving the performance of GO-reinforced polymer composites.

The XRD patterns (as shown in Figure 5) were analyzed to provide further evidence of modification. The XRD pattern of GO showed a sharp (002) diffraction peak at approximately 11°, corresponding to an interlayer spacing of 0.78 nm.[45,46] OAPS exhibited a strong diffraction peak at 8°, corresponding to a lattice spacing of 1 nm.[47] This diffraction peak could be attributed to the diameter of the OAPS cage, and similar results have been reported previously.[47,48] Furthermore, a broad peak was observed at 20° in the OAPS diffraction pattern, which was associated with the presence of amine substitutional isomers.[48] After modifying with OAPS, the (002) diffraction peak of GO disappeared in the OAPS-GO diffraction pattern, which only exhibited the weak intensity of the OAPS diffraction peaks. This result demonstrated that OAPS was intercalated into the GO sheets, increasing the interlayer distances and inducing ordered graphitic stacking of GO to well-disorder structures of OAPS-GO. Moreover, this result was also consistent with the result of a previous report.[42] Therefore, the presence of OAPS grafted onto the GO surface can restrain the restacking of the

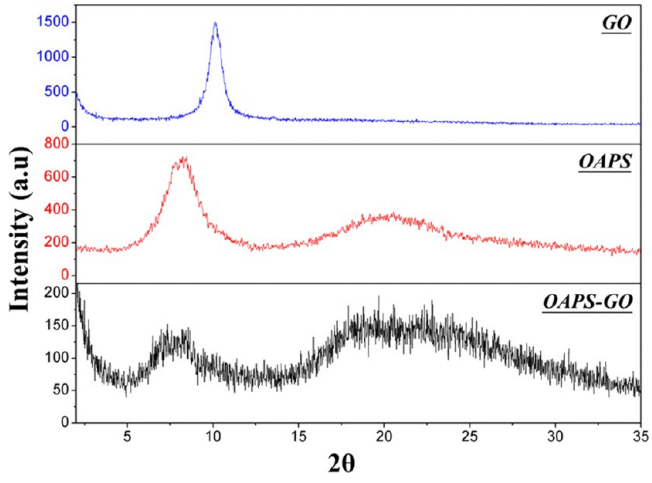

Figure 5. X-ray diffraction patterns of GO, OAPS, and OAPS-GO.

planar GO nanosheet, and form a disordered structure with low crystallinity.

Because different structural nanomaterials exhibit distinct thermal decomposition behaviors, TGA is a useful tool to investigate the thermal stability of the nanomaterials, and to measure the quantity of the substances grafted on GO (as shown in Figure 6). The TGA curve of OAPS exhibited a weight loss of approximately 60 wt % when the temperature increased from 450 to 700 °C, which was presumably associated with the thermal decomposition of aminophenyl in

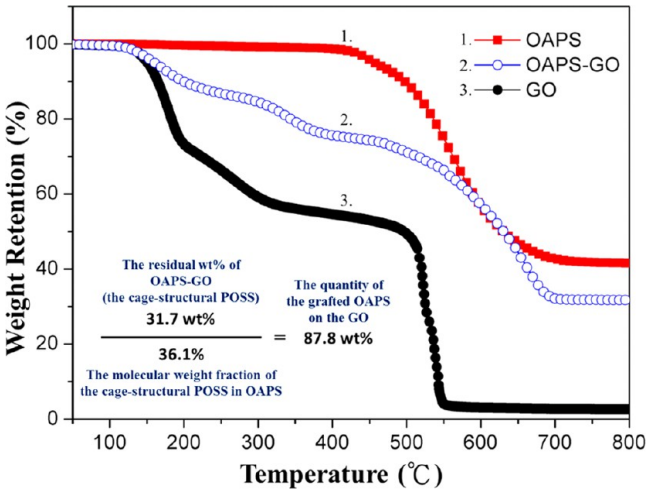

Figure 6. TGA curves of OAPS, GO, and OAPS-GO with a heating rate of 10 °C min^{-1} in air.

OAPS.[47] Because the molecular weight fraction of aminophenyl groups in OAPS is approximately 60 wt %, the residual 40 wt % corresponds to the thermally stable cage structure of POSS. GO undergoes a substantial weight loss at temperatures between 150 and 300 °C, which results from the reduction of oxygen-containing functional groups.[42,45] GO showed a slight weight loss at temperatures between 300 to 450 °C, which was attributed to defects such as disordered and amorphous carbon atoms in the graphene structure.[45,49] GO incurred complete thermal decomposition between 450 and 550 °C comprising the entire graphitic structure.[42,50] Compared with the thermal decomposition behaviors of OAPS and GO, OAPS-grafted GO sheets exhibited a substantially different weight loss curve and were thermally degraded in three stages. In the first stage, between 150 and 300 °C, weight loss was caused by the thermal degradation of the unreacted oxygen-containing functional groups of GO. In the second stage, from 300 to 450 °C, the TGA curve of OAPS-GO showed a slight weight loss, which was attributed to defects such as disordered and amorphous carbon atoms on the graphene structure. In the third stage, from 450 to 700 °C, a substantial weight loss was caused by the thermal degradation of aminophenylic groups in OAPS and complete thermal decomposition of GO. Furthermore, the quantity of the grafted OAPS on the GO sheets was estimated to be approximately 87.8 wt %. This estimation was determined by the residual 31.7 wt % of the cage-structural POSS and the

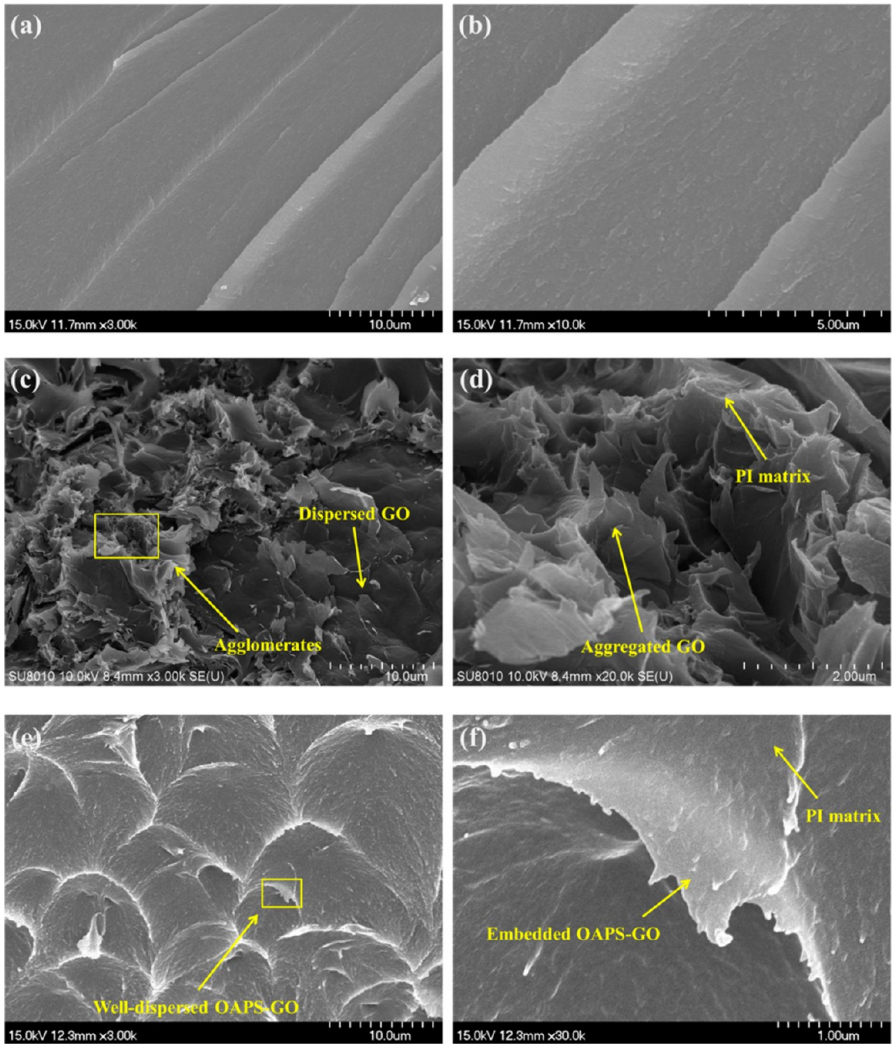

Figure 7. SEM images of fractured surface of (a) neat PI (×3k), (b) neat PI (×10k), (c) 3.0 wt % GO/PI film (×3k) and, (d) 3.0 wt % GO/PI film (×20k), (e) 3.0 wt % OAPS-GO/PI film (×10k), and, (f) 3.0 wt % OAPS-GO/PI film (×30k).

molecular weight fraction of the cage-structural POSS (36.1%) in OAPS, which was particularly close to the occupied content (89.6 wt %) of OAPS in OAPS-GO of the preparation process. The results demonstrated that the amine groups of OAPS substituted the epoxide groups of GO, modifying the GO surface properties successfully.

In summary, the results from XPS, TEM, XRD, and TGA analysis clearly showed that the GO sheets were functionalized by reaction of GO with OAPS successfully. It demonstrates that an effective method for producing OAPS-GO sheets, which can provide a versatile platform for fabricating polymer composites through in situ polymerization.

3.2. Morphology of the OAPS-GO/PI Composite Films. High-resolution SEM images of the fractured surfaces of the samples (as shown in Figure 7) were used to investigate the dispersion and compatibility of GO and OAPS-GO in a PI matrix, following tensile test. Images a and b in Figure 7 present the smooth surface of the neat PI, exhibiting the load-bearing unidirectional stripes. The SEM images of the GO/PI composite exhibited a heterogeneous surface with large agglomerates formed in the PI matrix (as shown in Figure 7c). To observe the morphology in detail, the partial area in Figure 7c was magnified as shown in Figure 7d. GO sheets exhibited poor compatibility with the PI matrix, and formed serious aggregation. This implies that pristine GO does not disperse effectively in the PI-precursor solution (PAA), resulted from the large surface area of GO, which stacks easily to form agglomerates. The GO agglomeration reduces the contact area between GO and PI, and results in the low GO-reinforcing efficiency. In contrast, incorporating OAPS-GO into the PI matrix (as shown in Figure 7e) resulted in the uniform augmentation of the roughness on the fractured surfaces of OAPS-GO/PI. To observe the morphology in detail, the partial area in Figure 7e was magnified as shown in Figure 7f. OAPS-GO was tightly embedded in the PI matrix, indicating the excellent compatibility of OAPS-GO in the PI matrix. To further demonstrate the dispersion of GO/PI and OAPS-GO/PI composites, TEM images of the 3.0 wt % GO/PI and the 3.0 wt % OAPS-GO/PI composites are provided in the Supporting Information. Consequently, the OAPS-GO surface with abundant amine-functional groups can not only achieve homogeneous dispersion of GO in the composite films effectively, but can also provide a starting platform for polymer grafting to construct strong interfaces between OAPS-GO and the PI matrix, thereby increasing the OAPS-GO-reinforcing efficiency in the mechanical properties of PI composites.

3.3. Mechanical Properties of the OAPS-GO/PI Composite Films. The reinforcing effects of the GO and OAPS-GO on the tensile properties of the PI composites are summarized in Figure 8 and Table 1. The tensile modulus of GO/PI composites increased from 2.20 to 3.28 GPa (approximately a 49% increase over neat PI film), and the tensile strength increased from 88.5 to 168.6 MPa (approximately a 91% increase over neat PI film) when the GO content increased from 0 to 1.0 wt %. Moreover, as the GO content increased from 1.0 to 3.0 and 5.0 wt %, the tensile modulus of the GO/PI composites increased to 6.25 and 7.29 GPa, respectively, but a decreasing trend was observed on the tensile strength of the GO/PI composites. This decreasing trend of the tensile strength was attributed to the filled GO reaching critical content,[6] and the distance between any two GO sheets being extremely short, causing van der Waals forces to become significant. Consequently, the GO agglomerated and restacked

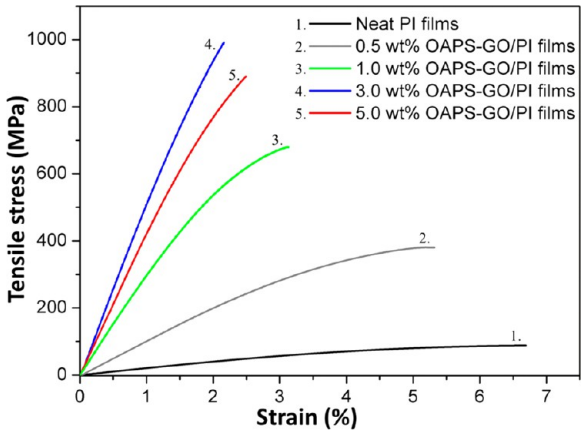

Figure 8. Stress–strain curves of neat PI films and OAPS-GO/PI films with various amounts of OAPS-GO.

Table 1. Mechanical Properties of Neat PI, GO/PI, and OAPS-GO/PI composites

sample	tensile modulus (GPa)	tensile strength (MPa)	elongation at break (%)
neat PI	2.20 ± 0.07	88.5 ± 6.1	6.69 ± 0.32
0.5 wt % GO/PI	3.28 ± 0.12	135.1 ± 9.5	5.52 ± 0.35
1.0 wt % GO/PI	4.63 ± 0.26	168.6 ± 10.4	4.82 ± 0.28
3.0 wt % GO/PI	6.25 ± 0.31	152.3 ± 12.6	4.55 ± 0.25
5.0 wt % GO/PI	7.29 ± 0.38	146.7 ± 10.2	4.28 ± 0.68
0.5 wt % OAPS-GO/PI	9.25 ± 0.56	378.6 ± 15.8	5.31 ± 0.42
1.0 wt % OAPS-GO/PI	15.6 ± 0.85	679.5 ± 36.1	3.13 ± 0.59
3.0 wt % OAPS-GO/PI	22.8 ± 0.92	986.8 ± 50.6	2.16 ± 0.55
5.0 wt % OAPS-GO/PI	21.6 ± 0.98	890.7 ± 58.2	2.49 ± 0.68

together (as observed in the SEM images of Figure 7c, d), which reduced the effective contact area between the GO surface and the PI polymer matrix.

As the OAPS-GO loading increased from 0 to 3.0 wt %, the tensile modulus and tensile strength increased from 2.20 GPa and 88.5 MPa to 22.8 GPa and 986.8 MPa, respectively. Compared with neat PI films, the OAPS-GO/PI composite film with only 3.0 wt % OAPS-GO exhibited a dramatic increase in tensile modulus (approximately 10.4 fold). In addition, 3.0 wt % OAPS-GO/PI possessed a substantial improvement in tensile strength (approximately 11.2 fold increase over neat PI film), revealing that OAPS-GO possessed a high reinforcing efficiency for promoting the load transfer from the polymer to OAPS-GO. This high-efficiency reinforcement might be attributable to the well-dispersed OAPS-GO in the polymeric matrix, as well as to the formation of strong interfaces between OAPS-GO and the PI matrix (as indicated in the SEM images of Figure 7e, f). Consequently, two reasons were proposed for the superior tensile properties of the OAPS-GO/PI composite films compared with GO/PI composites: (1) the grafted OAPS onto the GO surface can obtain a large interlayer spacing, preventing the restacking of the GO sheets, and (2) the OAPS-GO surface can provide abundant amine-functional groups for grafting PAA through the in situ polymerization. The grafted PI molecular chains on the OAPS-GO surface through covalent bonding caused a larger reinforcing zone and higher reinforcing efficiency than those of pristine GO in the PI matrix, which

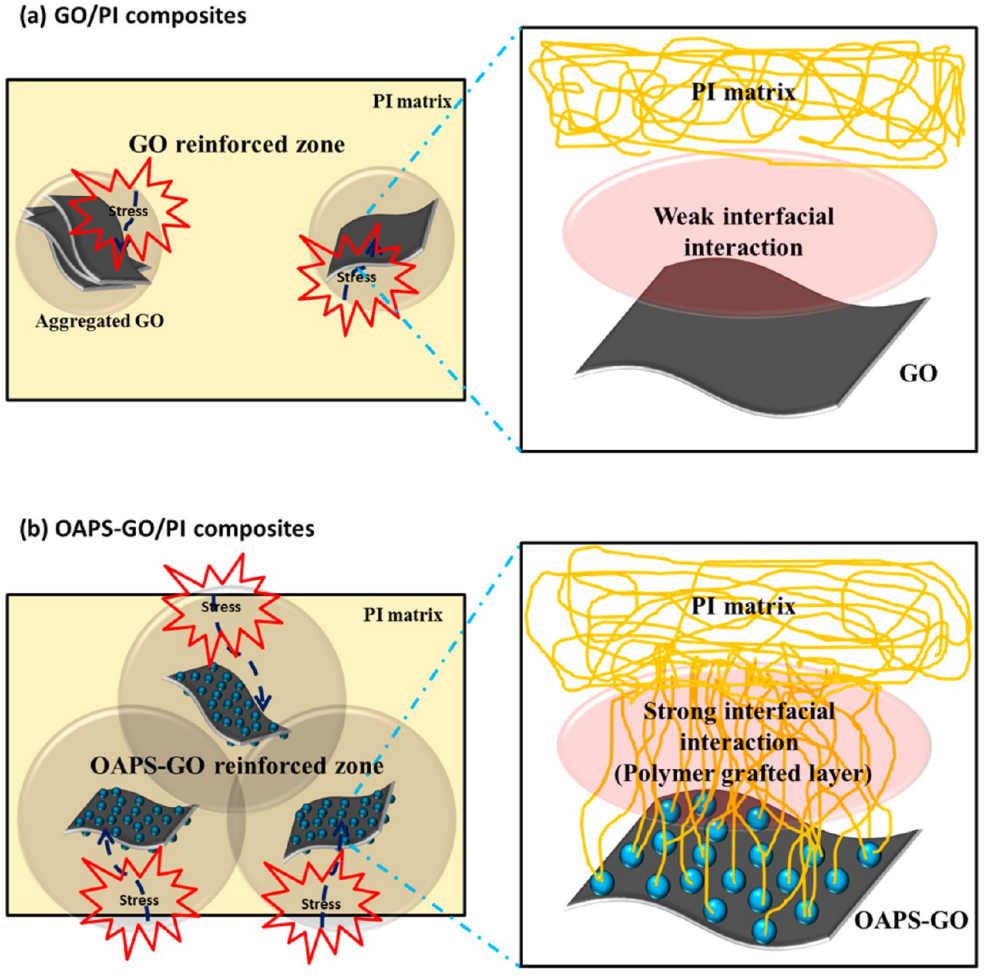

Figure 9. Proposed model of the reinforcing (a) GO and (b) OAPS-GO in PI polymeric matrix.

provides a high ability for transferring the stress from the PI polymeric matrix to OAPS-GO (as shown in Figure 9).

Furthermore, as the OAPS-GO content increased from 3.0 to 5.0 wt %, the reinforcing efficiency of OAPS-GO decreased slightly, and a similar trend was observed for the tensile modulus of the OAPS-GO/PI composite films. This indicates that the filler reached a critical content,[6] and the OAPS-GO sheets may agglomerate or restack, reducing the contact and reactive surface between OAPS-GO and PI, and the reinforcing efficiency of the mechanical properties was decreased. Therefore, an appropriate filler content of OAPS-GO can optimize the mechanical properties of the material. In summary, the OAPS-GO/PI composite films, which exhibited excellent tensile properties, suggest that OAPS-GO is an effective and versatile starting platform for preparing the PI composite films by using in situ polymerization.

3.4. Dielectric Properties of the OAPS-GO/PI Composite Films. The GO surface possesses a high density of oxygen-containing functional groups, which is an electrically insulating material.[17,51] These carbon−oxygen bonds were formed on the GO surface, and the sp^2-hybridized carbon atoms in graphite were transferred to the sp^3-hybridized carbon atoms in GO, causing the π-electrons were confined due to the incomplete conjugation. Because the D_k of air is approximately 1.0,[32] the nanoporous OAPS was grafted onto the GO surfaces to form OAPS-GO to achieve more insulating than GO. In this study, the insulating OAPS-GO sheets were introduced as interlayers in the PI matrix, restricting electron mobility in the OAPS-GO/PI composite.

Figure 10 presents the dielectric spectra of the neat PI films, the GO/PI composite films and the OAPS-GO/PI composite films, with the increasing of filler content (from 0.5 to 5.0 wt %), over a frequency range of 0.01 to 1 GHz. The neat PI films exhibited dielectric constants of approximately 3.3. The

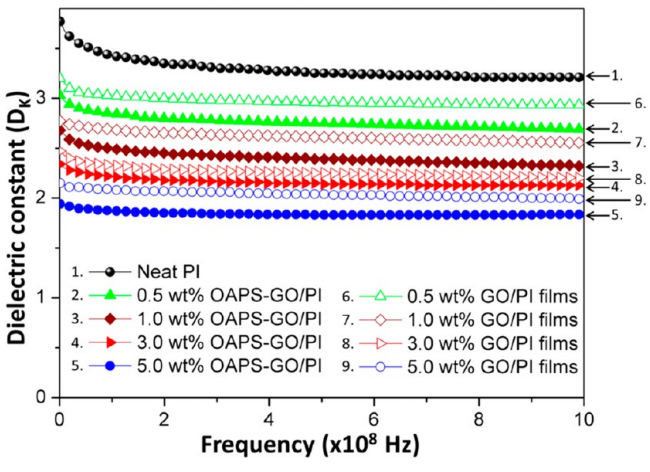

Figure 10. Dielectric constant as a function of frequency for neat PI films, OAPS-GO/PI films, and OAPS-GO/PI films.

dx.doi.org/10.1021/am504342j | ACS Appl. Mater. Interfaces 2014, 6, 15802−15812

dielectric constants of the PI composite films decreased with the addition of GO and OAPS-GO content, and the GO/PI films and OAPS-GO/PI films possessed significantly lower D_k values than that of neat PI. It is worth noting that the change in D_k is not proportional to the content of GO or OAPS-GO, and relatively large change occurs at the GO or OAPS-GO content below 1.0 wt %. Because the 2D layered structure and insulation of GO or OAPS-GO in the PI matrix may prevent the partial PI molecular chains from exhibiting the polarization effect[34] as the GO or OAPS-GO filler content is below 1.0 wt %, and the dielectric constants of the composites are considerably reduced. However, the other part of the PI molecular chains in these composites still encounters strong polarization effect. The quantity required for the GO or OAPS-GO sheets to effectively restrain the polarization effect in the PI molecular chains gradually trended toward saturation as the filler content surpassed 1.0 wt %. Therefore, the rate of D_k reduction in the composites at high filler contents is less than that of the composites at low filler contents; this phenomenon has also been observed in previous studies.[52−54] The dielectric constant of 5.0 wt % GO/PI films is approximately 2.1 (line 9 in Figure 10), and 5.0 wt % OAPS-GO/PI films achieved a D_k value of approximately 1.9 (line 5 in Figure 10). Compared with the GO/PI composite films, the OAPS-GO/PI composite films exhibited a greater reduction of the dielectric constant, indicating that the cage-structural OAPS with a nanoporous core (D_k of air is approximately 1.0.)[32] was grafted onto the GO surface, which could provide higher insulating properties than the pristine GO sheets could. This paper reports that the OAPS-GO/PI composite films with low D_k values can be fabricated through in situ polymerization, which had achieved the current requirement for ILD materials.

CONCLUSION

This paper demonstrates an effective method for preparing OAPS-GO/PI composite films with ultrastrong mechanical properties and a low dielectric constant. Results from XPS, TEM, XRD, and TGA analyses indicated that the GO sheets were successfully functionalized by the reaction with OAPS. The SEM result indicated that OAPS-GO not only exhibited excellent dispersibility and compatibility with the PI matrix, but also formed strong interfacial interactions with the PI polymeric chains. The 3.0 wt % OAPS-GO/PI composite films, prepared by in situ polymerization, exhibited an approximately 10.4-fold increase in tensile modulus, and a 11.2-fold increase in tensile strength. Furthermore, the bulk dielectric constant decreased from 3.3 for the neat PI film to 1.9 for the 5.0 wt % OAPS-GO/PI composite films. The performance of the OAPS-GO/PI composite films was substantially superior to that of the GO/PI composite films. Consequently, a 2D porous OAPS-GO was designed as a novel nanofiller to reinforce the polymeric matrix and provide an effective method for fabricating OAPS-GO/PI composite films with low dielectric constants and excellent mechanical properties for a wide range of applications.

ASSOCIATED CONTENT

Supporting Information

The surface morphologies, obtained using atomic force microscopy (AFM), consist of 2D- and 3D-AFM images and cross sections of GO and OAPS-GO. The percent compositions of the various functional groups for GO and OAPS-GO can be estimated from the peak area of the specific functional groups in the C 1s XPS spectrum. To investigate the difference between the OAPS-grafted GO by chemical bonding and the physical mixture of OAPS-adsorbed GO, TEM images of OAPS-adsorbed GO using the physical mixture method are provided. XPS was also used to investigate the OAPS-adsorbed GO, which was fabricated by the physical mixture method. ATR−FTIR studies of GO, OAPS and OAPS-GO were performed, and elucidated the chemical structure of surface modifiers through the analysis of the wavelength band of their vibration modes. Raman spectroscopy provided further evidence of OAPS grafting to GO. To further confirm the dispersibility of OAPS-GO in the PI matrix, TEM images of the GO/PI and OAPS-GO/PI composites are presented. This material is available free of charge via the Internet at http://pubs.acs.org/.

AUTHOR INFORMATION

Corresponding Author

*E-mail: ccma@che.nthu.edu.tw. Fax: 886-35715408.

Notes

The authors declare no competing financial interest.

ACKNOWLEDGMENTS

This work was supported by the Ministry of Science and Technology, Taipei, Taiwan, under Contracts 103-2221-E-007-001-(103) and 103-2221-E-007-130-(103). Boost Program from Low Carbon Energy Research Center of National Tsing Hua University is gratefully acknowledged.

REFERENCES

(1) Stankovich, S.; Dikin, D. A.; Dommett, G. H.; Kohlhaas, K. M.; Zimney, E. J.; Stach, E. A.; Piner, R. D.; Nguyen, S. T.; Ruoff, R. S. Graphene-Based Composite Materials. *Nature* **2006**, *442*, 282−6.

(2) Cai, D.; Song, M. Recent Advance in Functionalized Graphene/Polymer Nanocomposites. *J. Mater. Chem.* **2010**, *20*, 7906−7915.

(3) Rafiee, M. A.; Rafiee, J.; Wang, Z.; Song, H.; Yu, Z.-Z.; Koratkar, N. Enhanced Mechanical Properties of Nanocomposites at Low Graphene Content. *ACS Nano* **2009**, *3*, 3884−3890.

(4) Vleminckx, G.; Bose, S.; Leys, J.; Vermant, J.; Wübbenhorst, M.; Abdala, A. A.; Macosko, C.; Moldenaers, P. Effect of Thermally Reduced Graphene Sheets on the Phase Behavior, Morphology, and Electrical Conductivity in Poly[(α-methyl styrene)-co-(acrylonitrile)/poly(methyl-methacrylate) Blends. *ACS Appl. Mater. Interfaces* **2011**, *3*, 3172−3180.

(5) Yang, S.-Y.; Lin, W.-N.; Huang, Y.-L.; Tien, H.-W.; Wang, J.-Y.; Ma, C.-C. M.; Li, S.-M.; Wang, Y.-S. Synergetic Effects of Graphene Platelets and Carbon Nanotubes on the Mechanical and Thermal Properties of Epoxy Composites. *Carbon* **2011**, *49*, 793−803.

(6) Zhao, X.; Zhang, Q.; Chen, D.; Lu, P. Enhanced Mechanical Properties of Graphene-Based Poly(vinyl alcohol) Composites. *Macromolecules* **2010**, *43*, 2357−2363.

(7) Park, O.-K.; Hwang, J.-Y.; Goh, M.; Lee, J. H.; Ku, B.-C.; You, N.-H. Mechanically Strong and Multifunctional Polyimide Nanocomposites Using Amimophenyl Functionalized Graphene Nanosheets. *Macromolecules* **2013**, *46*, 3505−3511.

(8) Bose, S.; Khare, R. A.; Moldenaers, P. Assessing the Strengths and Weaknesses of Various Types of Pre-Treatments of Carbon Nanotubes on the Properties of Polymer/Carbon Nanotubes Composites: A Critical Review. *Polymer* **2010**, *51*, 975−993.

(9) Xu, Z.; Gao, C. In situ Polymerization Approach to Graphene-Reinforced Nylon-6 Composites. *Macromolecules* **2010**, *43*, 6716−6723.

(10) Xu, Y.; Liu, Z.; Zhang, X.; Wang, Y.; Tian, J.; Huang, Y.; Ma, Y.; Zhang, X.; Chen, Y. A Graphene Hybrid Material Covalently Functionalized with Porphyrin: Synthesis and Optical Limiting Property. *Adv. Mater.* **2009**, *21*, 1275−1279.

(11) Compton, O. C.; Dikin, D. A.; Putz, K. W.; Brinson, L. C.; Nguyen, S. T. Electrically Conductive "Alkylated" Graphene Paper via Chemical Reduction of Amine-Functionalized Graphene Oxide Paper. *Adv. Mater.* **2010**, *22*, 892−896.
(12) Figueiredo, J. L.; Pereira, M. F. R.; Freitas, M. M. A.; Órfão, J. J. M. Modification of the Surface Chemistry of Activated Carbons. *Carbon* **1999**, *37*, 1379−1389.
(13) Sharma, M.; Madras, G.; Bose, S. Cooperativity and Structural Relaxations in PVDF/PMMA Blends in the Presence of MWNTs: An Assessment through SAXS and Dielectric Spectroscopy. *Macromolecules* **2014**, *47*, 1392−1402.
(14) Pawar, S. P.; Pattabhi, K.; Bose, S. Assessing the Critical Concentration of NH_2 Terminal Groups on the Surface of MWNTs Towards Chain Scission of PC in PC/SAN Blends: Effect on Dispersion, Electrical Conductivity and EMI Shielding. *RSC Adv.* **2014**, *4*, 18842−18852.
(15) Mural, P. K. S.; Rana, M. S.; Madras, G.; Bose, S. PE/PEO Blends Compatibilized by PE Brush Immobilized on MWNTs: Improved Interfacial and Structural Properties. *RSC Adv.* **2014**, *4*, 16250−16259.
(16) Stankovich, S.; Piner, R. D.; Nguyen, S. T.; Ruoff, R. S. Synthesis and Exfoliation of Isocyanate-Treated Graphene Oxide Nanoplatelets. *Carbon* **2006**, *44*, 3342−3347.
(17) Dreyer, D. R.; Park, S.; Bielawski, C. W.; Ruoff, R. S. The Chemistry of Graphene Oxide. *Chem. Soc. Rev.* **2010**, *39*, 228−240.
(18) Li, D.; Kaner, R. B. Materials Science. Graphene-Based Materials. *Science* **2008**, *320*, 1170−1.
(19) Mkhoyan, K. A.; Contryman, A. W.; Silcox, J.; Stewart, D. A.; Eda, G.; Mattevi, C.; Miller, S.; Chhowalla, M. Atomic and Electronic Structure of Graphene-Oxide. *Nano Lett.* **2009**, *9*, 1058−1063.
(20) Park, S.; Lee, K.-S.; Bozoklu, G.; Cai, W.; Nguyen, S. T.; Ruoff, R. S. Graphene Oxide Papers Modified by Divalent Ions—Enhancing Mechanical Properties via Chemical Cross-Linking. *ACS Nano* **2008**, *2*, 572−578.
(21) Ramanathan, T.; Abdala, A. A.; Stankovich, S.; Dikin, D. A.; Herrera-Alonso, M.; Piner, R. D.; Adamson, D. H.; Schniepp, H. C.; Chen, X.; Ruoff, R. S.; Nguyen, S. T.; Aksay, I. A.; Prud'Homme, R. K.; Brinson, L. C. Functionalized Graphene Sheets for Polymer Nanocomposites. *Nat. Nanotechnol* **2008**, *3*, 327−31.
(22) Waddon, A. J.; Coughlin, E. B. Crystal Structure of Polyhedral Oligomeric Silsequioxane (POSS) Nano-materials: A Study by X-ray Diffraction and Electron Microscopy. *Chem. Mater.* **2003**, *15*, 4555−4561.
(23) Waddon, A. J.; Zheng, L.; Farris, R. J.; Coughlin, E. B. Nanostructured Polyethylene-POSS Copolymers: Control of Crystallization and Aggregation. *Nano Lett.* **2002**, *2*, 1149−1155.
(24) Kuo, S.-W.; Chang, F.-C. POSS related polymer nanocomposites. *Prog. Polym. Sci.* **2011**, *36*, 1649−1696.
(25) Zhang, W.; Müller, A. H. E. Architecture, Self-Assembly and Properties of Well-Defined Hybrid Polymers Based on Polyhedral Oligomeric Silsequioxane (POSS). *Prog. Polym. Sci.* **2013**, *38*, 1121−1162.
(26) Liang, K.; Li, G.; Toghiani, H.; Koo, J. H.; Pittman, C. U. Cyanate Ester/Polyhedral Oligomeric Silsesquioxane (POSS) Nanocomposites: Synthesis and Characterization†. *Chem. Mater.* **2005**, *18*, 301−312.
(27) Lee, Y.-J.; Huang, J.-M.; Kuo, S.-W.; Lu, J.-S.; Chang, F.-C. Polyimide and Polyhedral Oligomeric Silsesquioxane Nanocomposites for Low-Dielectric Applications. *Polymer* **2005**, *46*, 173−181.
(28) Maier, G. Low Dielectric Constant Polymers for Microelectronics. *Prog. Polym. Sci.* **2001**, *26*, 3−65.
(29) Maex, K.; Baklanov, M. R.; Shamiryan, D.; Iacopi, F.; Brongersma, S. H.; Yanovitskaya, Z. S. Low Dielectric Constant Materials for Microelectronics. *J. Appl. Phys.* **2003**, *93*, 8793−8841.
(30) Bohr, M. T. Interconnect Scaling−the Real Limiter to High Performance ULSI. In *Proceedings of the 1995 International Electron Devices Meeting*; Washington, D.C., Dec 10−13, 1995 ; IEEE: Piscataway, NJ, 1995; pp 241−244.
(31) Allan, A.; Edenfeld, D.; Joyner, W. H., Jr.; Kahng, A. B.; Rodgers, M.; Zorian, Y. 2001 technology roadmap for semiconductors. *Computer* **2002**, *35*, 42−53.
(32) Zhao, G.; Ishizaka, T.; Kasai, H.; Hasegawa, M.; Furukawa, T.; Nakanishi, H.; Oikawa, H. Ultralow-Dielectric-Constant Films Prepared from Hollow Polyimide Nanoparticles Possessing Controllable Core Sizes. *Chem. Mater.* **2008**, *21*, 419−424.
(33) Davis, M. E. Ordered Porous Materials for Emerging Applications. *Nature* **2002**, *417*, 813−821.
(34) Simpson, J. O.; Clair, A. K., St. Fundamental Insight on Developing Low Dielectric Constant Polyimides. *Thin Solid Films* **1997**, *308*−*309*, 480−485.
(35) Zhang, Y. H.; Lu, S. G.; Li, Y. Q.; Dang, Z. M.; Xin, J. H.; Fu, S. Y.; Li, G. T.; Guo, R. R.; Li, L. F. Novel Silica Tube/Polyimide Composite Films with Variable Low Dielectric Constant. *Adv. Mater.* **2005**, *17*, 1056−1059.
(36) Zhang, Y.-H.; Dang, Z.-M.; Fu, S.-Y.; Xin, J. H.; Deng, J.-G.; Wu, J.; Yang, S.; Li, L.-F.; Yan, Q. Dielectric and Dynamic Mechanical Properties of Polyimide−Clay Nanocomposite Films. *Chem. Phys. Lett.* **2005**, *401*, 553−557.
(37) Leu, C.-M.; Chang, Y.-T.; Wei, K.-H. Polyimide-Side-Chain Tethered Polyhedral Oligomeric Silsesquioxane Nanocomposites for Low-Dielectric Film Applications. *Chem. Mater.* **2003**, *15*, 3721−3727.
(38) Yu, W.; Fu, J.; Dong, X.; Chen, L.; Shi, L. A Graphene Hybrid Material Functionalized with POSS: Synthesis and Applications in Low-Dielectric Epoxy Composites. *Compos. Sci. Technol.* **2014**, *92*, 112−119.
(39) Valentini, L.; Bittolo Bon, S.; Cardinali, M.; Monticelli, O.; Kenny, J. M. POSS Vapor Grafting on Graphene Oxide Film. *Chem. Phys. Lett.* **2012**, *537*, 84−87.
(40) Valentini, L.; Cardinali, M.; Kenny, J. M.; Prato, M.; Monticelli, O. A Photoresponsive Hybrid Nanomaterial Based on Graphene and Polyhedral Oligomeric Silsesquioxanes. *Eur. J. Inorg. Chem.* **2012**, *2012*, 5282−5287.
(41) Valentini, L.; Bon, S. B.; Monticelli, O.; Kenny, J. M. Deposition of Amino-Functionalized Polyhedral Oligomeric Silsesquioxanes on Graphene Oxide Sheets Immobilized onto an Amino-Silane Modified Silicon Surface. *J. Mater. Chem.* **2012**, *22*, 6213−6217.
(42) Xue, Y.; Liu, Y.; Lu, F.; Qu, J.; Chen, H.; Dai, L. Functionalization of Graphene Oxide with Polyhedral Oligomeric Silsesquioxane (POSS) for Multifunctional Applications. *J. Phys. Chem. Lett.* **2012**, *3*, 1607−1612.
(43) Hummers, W. S.; Offeman, R. E. Preparation of Graphitic Oxide. *J. Am. Chem. Soc.* **1958**, *80*, 1339−1339.
(44) Tien, H.-W.; Hsiao, S.-T.; Liao, W.-H.; Yu, Y.-H.; Lin, F.-C.; Wang, Y.-S.; Li, S.-M.; Ma, C.-C. M. Using Self-Assembly to Prepare a Graphene-Silver Nanowire Hybrid Film that is Transparent and Electrically Conductive. *Carbon* **2013**, *58*, 198−207.
(45) Teng, C.-C.; Ma, C.-C. M.; Lu, C.-H.; Yang, S.-Y.; Lee, S.-H.; Hsiao, M.-C.; Yen, M.-Y.; Chiou, K.-C.; Lee, T.-M. Thermal Conductivity and Structure of Non-Covalent Functionalized Graphene/Epoxy Composites. *Carbon* **2011**, *49*, 5107−5116.
(46) Stankovich, S.; Dikin, D. A.; Compton, O. C.; Dommett, G. H. B.; Ruoff, R. S.; Nguyen, S. T. Systematic Post-assembly Modification of Graphene Oxide Paper with Primary Alkylamines. *Chem. Mater.* **2010**, *22*, 4153−4157.
(47) Choi, J.; Tamaki, R.; Kim, S. G.; Laine, R. M. Organic/Inorganic Imide Nanocomposites from Aminophenylsilsesquioxanes. *Chem. Mater.* **2003**, *15*, 3365−3375.
(48) Tamaki, R.; Choi, J.; Laine, R. M. A Polyimide Nanocomposite from Octa(aminophenyl)silsesquioxane. *Chem. Mater.* **2003**, *15*, 793−797.
(49) Liao, W.-H.; Tien, H.-W.; Hsiao, S.-T.; Li, S.-M.; Wang, Y.-S.; Huang, Y.-L.; Yang, S.-Y.; Ma, C.-C. M.; Wu, Y.-F. Effects of Multiwalled Carbon Nanotubes Functionalization on the Morphology and Mechanical and Thermal Properties of Carbon Fiber/Vinyl Ester Composites. *ACS Appl. Mater. Interfaces* **2013**, *5*, 3975−3982.
(50) Hsiao, M.-C.; Ma, C.-C. M.; Chiang, J.-C.; Ho, K.-K.; Chou, T.-Y.; Xie, X.; Tsai, C.-H.; Chang, L.-H.; Hsieh, C.-K. Thermally

Conductive and Electrically Insulating Epoxy Nanocomposites with Thermally Reduced Graphene Oxide−Silica Hybrid Nanosheets. *Nanoscale* **2013**, *5*, 5863−5871.
(51) Wang, Z.; Nelson, J. K.; Hillborg, H.; Zhao, S.; Schadler, L. S. Graphene Oxide Filled Nanocomposite with Novel Electrical and Dielectric Properties. *Adv. Mater.* **2012**, *24*, 3134−3137.
(52) Lin, J.; Wang, X. Novel Low-κ Polyimide/Mesoporous Silica Composite Films: Preparation, Microstructure, and Properties. *Polymer* **2007**, *48*, 318−329.
(53) Leu, C.-M.; Chang, Y.-T.; Wei, K.-H. Synthesis and Dielectric Properties of Polyimide-Tethered Polyhedral Oligomeric Silsesquioxane (POSS) Nanocomposites via POSS-diamine. *Macromolecules* **2003**, *36*, 9122−9127.
(54) Wang, J.-Y.; Yang, S.-Y.; Huang, Y.-L.; Tien, H.-W.; Chin, W.-K.; Ma, C.-C. M. Preparation and Properties of Graphene Oxide/Polyimide Composite Films with Low Dielectric Constant and Ultrahigh Strength via In Situ Polymerization. *J. Mater. Chem.* **2011**, *21*, 13569−13575.